computation

MDPI

*Article*

# Space-Time Primal-Dual Active Set Method: Benchmark for Collision of Elastic Bar with Discontinuous Velocity

**Victor A. Kovtunenko** [1,2]

[1] Department of Mathematics and Scientific Computing, Karl-Franzens University of Graz, NAWI Graz, Heinrichstr. 36, 8010 Graz, Austria; victor.kovtunenko@uni-graz.at
[2] Lavrentyev Institute of Hydrodynamics, Siberian Division of the Russian Academy of Sciences, 630090 Novosibirsk, Russia

**Abstract**

The dynamic contact problem describing collision of an elastic bar with a rigid obstacle, prescribed by an initial velocity, is considered in a variational formulation. The non-smooth, piecewise-linear solution is constructed analytically using partition of a 2D rectangular domain along characteristics. Challenged by the discontinuous velocity after collision, full discretization of the problem is applied that is based on a space-time finite element method. For an iterative solution of the discrete variational inequality, a primal–dual active set algorithm is used. Computer simulation of the collision problem is presented on uniform triangle grids. The active sets defined in the 2D space-time domain converge in a few iterations after re-initialization. The benchmark solution at grid points is indistinguishable from the analytical solution. The discrete energy has no dissipation, it is free of spurious oscillations, and it converges super-linearly under mesh refinement.

**Keywords:** impact contact dynamics; variational inequality; discontinuous velocity; space-time finite element; primal-dual active set

**MSC:** 35L85; 49M15; 74S05

check for updates

Academic Editor: Demos T. Tsahalis

Received: 31 July 2025
Revised: 15 August 2025
Accepted: 18 August 2025
Published: 1 September 2025

**Citation:** Kovtunenko, V.A. Space-Time Primal-Dual Active Set Method: Benchmark for Collision of Elastic Bar with Discontinuous Velocity. *Computation* **2025**, *13*, 210. https://doi.org/10.3390/computation13090210



## 1. Introduction

In this paper, the research aims at solutions of dynamic contact problems, which model the time-dependent deformation of a solid body colliding a rigid obstacle. The moving body and the stationary obstacle have different velocities, therefore, an impact occurs. By using elementary physics concepts, some elastic properties of falling bars and springs that were suddenly released after being hung from one end were discussed in [1]. In experiments of body motion, a spring allowed larger deformations and slower wave propagation than an elastic bar. Highlighting broader relevance in variational mechanics, this work cites studies on nonlinear vibrations and micro-electro-mechanical systems (MEMSs) involving micro-beams and sensors [2]. The periodic motion of an MEMS is highly sensitive to operating conditions and may become unstable when reaching specific threshold values [3]. This makes it crucial to find an exact solution of the problem and to gain insight the property of dynamic stability, which is highly important for numerical solution.

Since responses by the impact demonstrate an oscillatory nature, proper solution methods of contact dynamics problems should follow its wave propagation characteristics. The mathematical analysis of solutions to variational and hemivariational inequalities describing contact problems can be found in [4,5]. The solvability to wave equations stated in half-space

under unilateral constraints imposed at the boundary was proved in [6]. This work refers to monographs [7,8] for the basic computational concepts used in the field, to [9,10] for finite element methods (FEM), and to [11,12] for boundary element methods (BEM). For some dynamic issues in physical modeling this work cites [13–19] for bio-mechanical models.

To illustrate properties of colliding bodies, this study performs theoretical analysis and numerical simulation of the dynamic contact problem in a two-dimensional (2D) setting. In our context, one dimension is time, and the second dimension is space. For benchmark, this work considers a 1D elastic bar of the prescribed initial position and initial velocity, for which an exact solution is derived. The bar undergoes a rigid body motion until its end collides with the rigid obstacle. Is stays in contact during elastic waves travel through the body and then moves back as the waves reach the bar end. This benchmark of collision is relevant to the considerations from [20,21], where an undeformed bar was dropped against a rigid ground surface with a given initial velocity. In the other relevant benchmark from [22–24], a rigid obstacle was impacted by an initially deformed elastic bar with zero initial velocity.

From the mathematical point of view, the impact of bodies is characterized by a discontinuous velocity; see [25]. For time integration, there are the well-established semi-discrete methods of Newmark [26] and Hilber–Hughes–Taylor [27]. For extension of the HHT method to dynamic contact problems within a semi-smooth Newton approach, the reader is referred to [28–30]. However, when determining the acceleration from an expansion in Taylor series, these numerical integration schemes assume continuity of velocity. The variational theory of discontinuous solutions to problems stated in non-smooth domains was elaborated in [31,32] and relevant works [33–36]. The reader is referred to proper numerical methods in [37–39] and to asymptotic methods using boundary layers in [40–42].

For efficient iterative solution of complementarity problems, there are well-known semi-smooth Newton (SSN) methods, which have a locally super-linear convergence rate. Moreover, the realization of SSN methods as a primal–dual active set (PDAS) iteration converges globally in a monotone way for stiffness matrices obeying the M-matrix property; see [43]. The a priori and a posteriori numerical analysis of PDAS algorithms for static unilaterally constrained problems in mechanics was given in [44,45]. In the theory of dynamic multi-body and discrete contact problems, for the realization of the PDAS strategy and corresponding numerical simulations, this work refers to [46,47].

To take the velocity discontinuity into account, in [48,49], we first realized a space-time PDAS approach, which is based on a full discretization of dynamic variational inequalities within space-time finite elements, referred to here as ST-PDAS for short. The reader can find studies of the space-time approximation for second-order hyperbolic equations in [50,51]. Unconditionally stable conforming finite element discretization with piecewise polynomial functions in space and time was studied in the literature performing continuous solutions for heat and wave equations. In constrast, this study's contribution to the field pays attention to solutions with discontinuous derivatives offering analytical–numerical synergy of impact phenomena. In this research's previous works, the dynamic contact condition was stated at a 1D boundary. In contrast, in the current contribution, this study presents contact sets over the whole 2D space-time domain. The novelty consists in developing the ST-PDAS algorithm for contact conditions imposed in two dimensions. This study constructs an analytical benchmark of non-smooth solutions of the wave equation, which is given by piecewise linear functions along characteristics on a suitable partition of rectangular domains.

In Section 2, the collision problem is formulated as a variational inequality for the wave equation given in a rectangle and subject to a one-sided inequality constraint. The analytical solution having discontinuous time and spatial derivatives is proven in Section 3. For its numerical realization, in Section 4, the problem within ST-FEM is approximated by

piecewise linear polynomial functions on uniform triangular grids, and it is solved with the help of PDAS. In Section 5, numerical experiments of the benchmark are presented, and properties of the full approximation are discussed. Namely, the ST-PDAS algorithm converges in only few iterations; its numerical solution almost coincides with the analytical solution at grid points. The discrete energy is non-dissipative and converges super-linearly when the mesh size decreases.

## 2. Formulation of the Collision Problem

In the following, we neglect the force of gravity for simplicity. We consider a bar of length $L > 0$ made of a linear elastic isotropic material of unit density and unit modulus of rigidity. In the undeformed configuration $x \in (0, L)$, where $t = 0$, let the bar be posed below the origin at initial depth $H > 0$ without initial deformation. Pushed with an initial velocity $v_0 > 0$, Figure 1 illustrates motion of the bar in the deformed configuration $x + u(t, x)$.

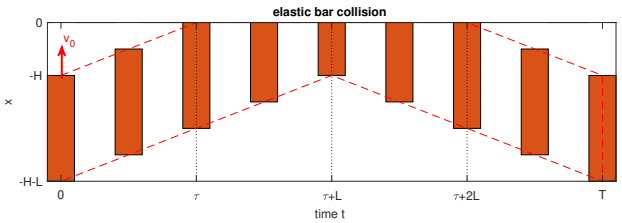


**Figure 1.** The collision benchmark in the deformed configuration $x + u(t, x)$ for $(t, x) \in Q$.

Its displacement $u(t, x)$ in the rectangle $Q = (0, T) \times (0, L)$ with the boundary $\partial Q$, defined for some fixed final time $T > 0$, is described by the inhomogeneous wave equation:

$$u_{tt}(t, x) - u_{xx}(t, x) = \lambda(t, x) \quad \text{for } (t, x) \in Q, \tag{1}$$

where $\lambda$ is a contact force such that

$$\lambda(t, L) = u_x(t, L) \quad \text{for } t \in (0, T). \tag{2}$$

Here, $u_{tt}$ stands for the second time derivative (the acceleration) $u_x$ and $u_{xx}$ for the first and second space derivatives, respectively. The equation of motion (1) is supported by the following initial conditions:

$$u(0, x) = 0, \quad u_t(0, x) = v_0 \quad \text{for } x \in (0, L), \tag{3}$$

where $u_t$ is the first time derivative (the velocity). Let the lower bar end $x = 0$ be free and defined as

$$u_x(t, 0) = 0 \quad \text{for } t \in (0, T), \tag{4}$$

where $u_x$ denotes the first space derivative.

The upper end $x = L$ collides with the rigid obstacle occupying the half-space $x \geq 0$. Therefore, the following complementarity conditions should hold for all space-time points:

$$u(t, x) \leq L - x, \quad \lambda(t, x) \leq 0, \quad \lambda(t, x)\big(u(t, x) - L + x\big) = 0 \quad \text{for } (t, x) \in \widetilde{Q} \tag{5}$$

on the set $\widetilde{Q} = Q \cup \Gamma$, where $\Gamma = \{t \in (0, T),\ x = L\}$. In (5), the former inequality yields non-penetration over the obstacle, that is, $u(t, L) \leq 0$ at the upper end $x = L$ and $u(t, 0) \leq L$ approaching the lower end $x = 0$ of the bar. Under contact, the force should be non-expansive; hence, $\lambda$ is non-positive. The non-penetration equations and inequalities (5) imply that $u(t, x) \leq L - x$ and $\lambda(t, x) = 0$ before and after collision; otherwise, $u(t, x) = L - x$ and $\lambda(t, x) \leq 0$ during the collision.

**Remark 1.** *By continuity, the non-penetration condition $u(t,x) \le L - x$ can be extended to the the closure* $\mathrm{cl}(Q) = Q \cup \partial Q$.

**Remark 2.** *For comparison, if contact conditions* (2) *and* (5) *are stated at the boundary portion* $\Gamma$ *only, then they turn into the complementarity relations:*

$$\lambda(t,L) = u_x(t,L), \quad u(t,L) \le 0, \quad \lambda(t,L) \le 0, \quad \lambda(t,L)u(t,L) = 0 \quad \text{for } t \in (0,T). \tag{6}$$

*The particular case* (6) *can be treated as described in the previous works* [48,49].

After integration by parts using Green's formula for smooth functions $u, v$ in $\mathrm{cl}(Q)$, we have

$$\int_Q (u_{tt} - u_{xx}) v \, dxdt = \int_Q (-u_t v_t + u_x v_x) \, dxdt + \int_0^L u_t v \, dx\big|_{t=0}^T - \int_0^T u_x v \, dt\big|_{x=0}^L \tag{7}$$

and we give a weak formulation to the initial boundary value problems (1)–(5). For this task, the following notation of linear sub-spaces from [50] is employed:

$$H^1_{0,}(0,T) = \{v \in H^1(0,T),\, v(0) = 0\}, \quad H^1_{,0}(0,T) = \{v \in H^1(0,T),\, v(T) = 0\}.$$

We look for a solution $u \in V_{0,}$ from the trial space

$$V_{0,} = L^2(0,T; H^1_{0,}(0,L)) \cap H^1_{0,}(0,T; L^2(0,L))$$

such that $u(t,x) \le L - x$ for $(t,x) \in \widetilde{Q}$, which satisfies the following variational inequality:

$$\int_Q \big(-u_t(v_t - u_t) + u_x(v_x - u_x)\big) \, dxdt \ge \int_0^L v_0 v \, dx\big|_{t=0} \tag{8}$$

for all functions $v - u \in V_{,0}$ such that $v(t,x) \le L - x$, for $(t,x) \in \widetilde{Q}$, from the test space

$$V_{,0} = L^2(0,T; H^1_{0,}(0,L)) \cap H^1_{,0}(0,T; L^2(0,L)).$$

Conversely, if the variational solution to (8) is smooth such that $u, u_x \in C(\mathrm{cl}(Q))$, then the Green Formula (7) justifies the initial boundary value problems (1)–(5).

The variational inequality (8) can be rewritten as the following system of primal and dual relations: Find solution pair $(u,\lambda) \in V_{0,} \times L^2(Q) \bigcup L^2(\Gamma)$ such that

$$\begin{gathered} u \le L - x, \quad \lambda \le 0 \quad \text{in } \widetilde{Q}, \quad \int_Q \lambda(u - L + x) \, dxdt + \int_0^T \lambda u \, dt\big|_{x=L} = 0, \\ \int_Q (-u_t v_t + u_x v_x) \, dxdt = \int_0^L v_0 v \, dx\big|_{t=0} + \int_Q \lambda v \, dxdt + \int_0^T \lambda v \, dt\big|_{x=L} \end{gathered} \tag{9}$$

for all test functions $v \in V_{,0}$. Indeed, introducing the contact force $\lambda$ according to Equations (1) and (2) and using Green's Formula (7) for $v - u$ yields

$$\begin{aligned} &\int_Q \lambda(v - u) \, dxdt = \int_Q (u_{tt} - u_{xx})(v - u) \, dxdt \\ &= \int_Q \big(-u_t(v_t - u_t) + u_x(v_x - u_x)\big) \, dxdt + \int_0^L u_t(v - u) \, dx\big|_{t=0}^T - \int_0^T u_x(v - u) \, dt\big|_{x=0}^L \\ &= \int_Q \big(-u_t(v_t - u_t) + u_x(v_x - u_x)\big) \, dxdt - \int_0^L v_0 v \, dx\big|_{t=0} - \int_0^T \lambda(v - u) \, dt\big|_{x=L}. \end{aligned}$$

Through the variational inequality (8), it follows that

$$\int_Q \lambda\big(v - L + x - (u - L + x)\big)\, dxdt + \int_0^T \lambda(v - u)\, dt\big|_{x=L} \geq 0$$

for all functions such that $v \leq L - x$ in $\widetilde{Q}$. These relations imply the primal–dual system (9).

Conversely, testing (9) with $v - u \in V_{,0}$, we derive that

$$\begin{aligned}
&\int_Q \big(-u_t(v_t - u_t) + u_x(v_x - u_x)\big)\, dxdt \\
&= \int_0^L v_0(v - u)\, dx\big|_{t=0} + \int_Q \lambda\big(v - L + x - (u - L + x)\big)\, dxdt + \int_0^T \lambda(v - u)\, dt\big|_{x=L} \\
&= \int_0^L v_0 v\, dx\big|_{t=0} + \int_Q \lambda(v - L + x)\, dxdt + \int_0^T \lambda v\, dt\big|_{x=L}.
\end{aligned}$$

It follows the variational inequality (8) if $\lambda(t,x) \leq 0$ and $v(t,x) \leq L - x$ for $(t,x) \in \widetilde{Q}$.

## 3. Analytical Solution to the Variational Inequality

Below, an analytical solution to the variational inequality (8) is provided drawn in three plots of Figure 2: the displacement $u(t,x)$, velocity $u_t(t,x)$, and space derivative $u_x(t,x)$ for $(t,x) \in \mathrm{cl}(Q)$. The piecewise linear solution is constructed explicitly along characteristics $x + t =$const before collision, which begins at the time $\tau = H/v_0$ and along $x - t =$const afterwords. By this, the time and space derivatives are discontinuos across the characteristics $x + t = \tau + L$ and $x - t = -\tau - L$. The magnitudes of the velocity $u_t$ and the gradient $u_x$ discontinuities equal $v_0$.

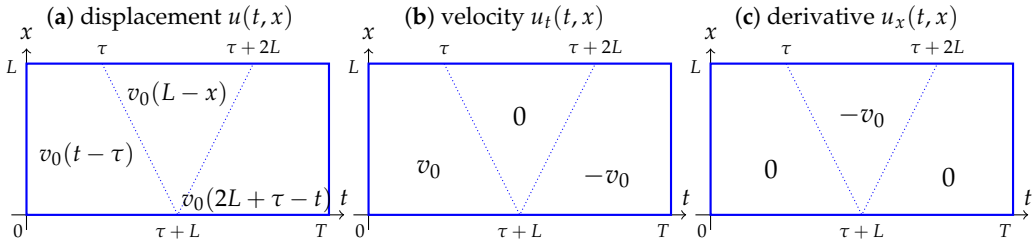


**Figure 2.** Analytical solution: displacement (**a**); velocity (**b**); space derivative (**c**).

**Theorem 1.** *Let the final time be $T \geq \tau + 2L$ and the initial velocity be $v_0 \leq 1$. Set the partition $\mathrm{cl}(Q) = \bigcup_{i=1}^3 K_i$, where*

$$\begin{aligned}
K_1 &= \{(t,x) \in \mathrm{cl}(Q) :\ x + t \leq \tau + L\}, \\
K_2 &= \{(t,x) \in \mathrm{cl}(Q) :\ x + t \geq \tau + L,\ x - t \geq -\tau - L\}, \\
K_3 &= \{(t,x) \in \mathrm{cl}(Q) :\ x - t \leq -\tau - L\}.
\end{aligned} \tag{10}$$

*A unique solution to the variational inequality (8) is given by*

$$u(t,x) = \begin{cases} v_0(t - \tau) & \text{in } K_1, \\ v_0(L - x) & \text{in } K_2, \\ v_0(\tau + 2L - t) & \text{in } K_3. \end{cases} \tag{11}$$

**Proof.** For the elements $K_1$–$K_3$ in the partition (10), let us denote by $\Gamma_{12}$ the joint side between $K_1$ and $K_2$ with the normal $(1,1)/\sqrt{2}$ and by $\Gamma_{23}$ the interface between $K_2$ and $K_3$ with the normal $(1,-1)/\sqrt{2}$. The jump of a discontinuous field $w(t,x)$ is denoted by

$$[\![w]\!] = w\big|_{\partial K_2 \cap \Gamma_{12}} - w\big|_{\partial K_1 \cap \Gamma_{12}}, \quad [\![w]\!] = w\big|_{\partial K_3 \cap \Gamma_{23}} - w\big|_{\partial K_2 \cap \Gamma_{23}}.$$

We apply to the elements in partition the Green Formula (7) written for piecewise smooth functions $u, v$ with discontinuous derivatives such that

$$\begin{aligned}\sum_{i=1}^{3} \int_{K_i} (u_{tt} - u_{xx}) v \, dxdt = \sum_{i=1}^{3} \int_{K_i} (-u_t v_t + u_x v_x) \, dxdt \\ - \int_{\Gamma_{12}} [\![(u_t - u_x)v]\!] \frac{1}{\sqrt{2}} \, d\Gamma - \int_{\Gamma_{23}} [\![(u_t + u_x)v]\!] \frac{1}{\sqrt{2}} \, d\Gamma \\ + \int_0^L u_t v \, dx\big|_{t=0}^{T} - \int_0^T u_x v \, dt\big|_{x=0}^{L}.\end{aligned} \tag{12}$$

The piecewise linear function in (11) is continuous and satisfies the following relations:

$$\begin{cases} u_{tt} = u_{xx} = 0 & \text{in } K_1\text{–}K_3, \\ [\![u_t]\!] = [\![u_x]\!] = -v_0 & \text{on } \Gamma_{12}, \\ [\![u_t]\!] = -v_0, \quad [\![u_x]\!] = v_0 & \text{on } \Gamma_{23}, \\ u_t\big|_{t=0} = v_0, \quad u_x\big|_{x=0} = 0 & \text{on } \partial Q, \\ u(t,L) = v_0(t-\tau), \quad u_x(t,L) = 0 & \text{for } t \in [0,\tau], \\ u(t,L) = 0, \quad u_x(t,L) = -v_0 & \text{for } t \in [\tau, \tau+2L], \\ u(t,L) = v_0(2L+\tau-t), \quad u_x(t,L) = 0 & \text{for } t \in [\tau+2L, T]. \end{cases} \tag{13}$$

Inserting (13) into (12) with smooth functions $v$ such that $[\![(u_t - u_x)v]\!] = [\![u_t - u_x]\!]v$ at $\Gamma_{12}$ and $[\![(u_t + u_x)v]\!] = [\![u_t + u_x]\!]v$ at $\Gamma_{23}$ yields the variational equation

$$\begin{aligned}\int_Q (-u_t v_t + u_x v_x) \, dxdt - \int_0^L v_0 v \, dx\big|_{t=0} = \int_0^T u_x v \, dt\big|_{x=L} \\ = -\int_\tau^{\tau+2L} v_0 v \, dt\big|_{x=L} \geq 0\end{aligned} \tag{14}$$

for all functions $v \in V_{,0}$ such that $v(t,L) \leq 0$ for $t \in (\tau, \tau+2L)$. In particular, testing (14) with $v = u\chi$, where a cutoff function $\chi(t)$ is compactly supported in $(0,T)$ and $\chi(t) = 1$ for $t \in (0, T-\zeta)$ with small $\zeta > 0$, we get the identity

$$\int_Q \big(-u_t (u\chi)_t + u_x u_x \chi\big) \, dxdt = \int_0^T u_x u \chi \, dt\big|_{x=L} = 0. \tag{15}$$

The subtraction of (15) from (14) leads to the following variational inequality

$$\int_Q \big(-u_t (v_t - u_t) + u_x (v_x - u_x)\big) \, dxdt \geq \int_0^L v_0 v \, dx\big|_{t=0} \tag{16}$$

which holds for all test functions $v - u \in V_{,0}$ such that $v(t,L) \leq 0$ for $t \in (0,T)$.

Moreover, the function in (11) justifies the following equations on the partition:

$$\begin{cases} u - L + x = (v_0 - 1)(t-\tau) + x + t - \tau - L, \quad u_x(t,L) = 0 & \text{in } K_1, \\ u - L + x = (v_0 - 1)(L - x), \quad u_x(t,L) = -v_0 & \text{in } K_2, \\ u - L + x = (v_0 - 1)(2L + \tau - t) + x - t + \tau + L, \quad u_x(t,L) = 0 & \text{in } K_3. \end{cases} \tag{17}$$

For $t \leq \tau$, the position yields $u - L + x = v_0(t - \tau) - L + x \leq 0$ in (11) for all points $x \leq L$. Let $v_0 - 1 \leq 0$ in (17). Then, $u - L + x = (v_0 - 1)(t - \tau) + x + t - \tau - L \leq 0$ for $t \geq \tau$ and $x + t - \tau - L \leq 0$ in $K_1$. In $K_2$, there holds $u - L + x = (v_0 - 1)(L - x) \leq 0$ for all $x \leq L$. If $t \leq \tau + 2L$ and $x - t + \tau + L \leq 0$, then $u - L + x = (v_0 - 1)(2L + \tau - t) + x - t + \tau + L \leq 0$ in $K_3$. For all $t \geq \tau + 2L$, we have $u - L + x = v_0(2L + \tau - t) \leq 0$ in (11). Therefore, the non-penetration condition $u(t, x) \leq L - x$ holds globally. To fulfill with (17) the complementarity conditions (5), we set a discontinuous contact force in the following form:

$$\lambda(t, x) = \begin{cases} 0 & \text{in } Q, \\ u_x & \text{on } \Gamma. \end{cases} \tag{18}$$

The uniqueness of solution to the problem (8) follows by an energy method. □

**Remark 3.** *The function pair* $(u, \lambda)$ *defined in* (11) *and* (18) *solves the primal–dual problem* (9).

**Remark 4.** *The global solution in* (11) *holds true when restricted for smaller values* $T < \tau + 2L$, *also for larger velocities* $v_0 > 1$ *within the time* $t \in (0, \tau)$, *when* $u - L + x \leq 0$ *in* (17).

Next, we consider the time-dependent energy of the bar as

$$E(t) = \frac{1}{2} \int_0^L (u_t^2 + u_x^2)\, dx, \quad t \in [0, T]. \tag{19}$$

Since the collision is supposed to be elastic, the energy is conserved, as justified below.

**Corollary 1.** *Under the assumptions of Theorem 1, the energy defined in* (19) *remains constant in time as*

$$E(t) = E(0) = \frac{1}{2} L v_0^2 \quad \text{for } t \in [0, T]. \tag{20}$$

**Proof.** Consider the intersection of elements $K_1$–$K_3$ from (10) with the rectangle $[0,\, s] \times [0,\, L]$ at fixed $s \in [0,\, T]$. We test with the discontinuous function $v = u_t$ the Green Formula (12) and skip integration by parts over time to calculate the following expression:

$$\begin{aligned} \sum_{i=1}^{3} \int_{K_i \cap \{t<s\}} (u_{tt} - u_{xx}) u_t \, dxdt &= \frac{1}{2} \sum_{i=1}^{3} \int_{K_i \cap \{t<s\}} (u_t^2 + u_x^2)_t \, dxdt \\ + \int_{\Gamma_{12} \cap \{t<s\}} [\![ u_x u_t ]\!] \frac{1}{\sqrt{2}} \, d\Gamma - \int_{\Gamma_{23} \cap \{t<s\}} [\![ u_x u_t ]\!] \frac{1}{\sqrt{2}} \, d\Gamma &- \int_0^s u_x u_t \, dt \Big|_{x=0}^{L}. \end{aligned} \tag{21}$$

Using properties (13) and zero product $u_x u_t = 0$ in $K_1$–$K_3$, integration of (21) by parts over time yields

$$\begin{aligned} 0 = \frac{1}{2} \sum_{i=1}^{3} \int_{K_i \cap \{t<s\}} (u_t^2 + u_x^2)_t \, dxdt &= E\big|_{t=0}^{s} - \frac{1}{2} \int_{(\Gamma_{12} \cup \Gamma_{23}) \cap \{t<s\}} [\![ u_t^2 + u_x^2 ]\!] \frac{1}{\sqrt{2}} \, d\Gamma \\ &= E\big|_{t=0}^{s} \end{aligned}$$

due to $u_t^2 + u_x^2 = v_0^2$ in $K_1$–$K_3$. This identity and $E(0) = L v_0^2/2$ prove the assertion (20). □

In the next section, we discretize the primal–dual problem (9) by using ST-FEM approach on a uniform triangular mesh, and we adapt PDAS for its numerical solution.

## 4. ST-PDAS Approximation

Let $\mathrm{cl}(Q) = \bigcup_{i\in I} T_i$ be divided into equal triangles $T_i$ indexed by a set $I$ comprising a uniform grid of size $h > 0$, where $h = 1/(N-1)$ for prescribed $N \in \mathbb{N}$. The grid nodes $(t_h, x_h) = \{(t_j, x_j)\}$ account for the number of degrees of freedom DOF $= (T/h+1)(L/h+1)$, with the number $M = (T/h-1)L/h$ of nodes $(t_h, x_h) \in \widetilde{Q}$. For $T = 4$ and $L = 1$, an example grid with $h = 0.25$ constituting DOF=85 and $M = 60$ is shown in Figure 3: before deformation in the left plot (a) and after deformation in the right plot (b). A full space-time discretization of the variational problem in the space of continuous piecewise linear functions is introduced below:

$$V^h = \{v_h \in C(\mathrm{cl}(Q)), \quad v_h|_{T_i} \in \mathbb{P}_1(T_i)^2 \text{ for } i \in I\},$$

where the trial $V_{0,}$ and the test $V_{,0}$ spaces are respectively,

$$V^h_{0,} = \{v_h \in V^h,\ v_h(0,\cdot) = 0\}, \quad V^h_{,0} = \{v_h \in V^h,\ v_h(T,\cdot) = 0\}.$$

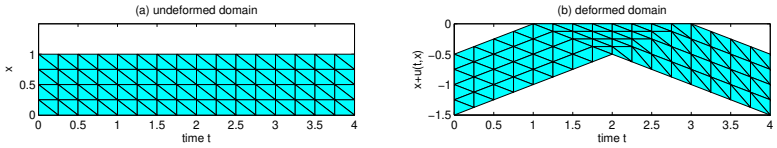


**Figure 3.** The diagonal triangle grid for $N = 5$ before deformation (**a**) and after deformation (**b**).

Let us denote by $\phi_h = \{\phi_j\}$, $j = 1, \ldots$,DOF, standard hat functions spanning the nodal basis in $V^h$ such that each $\phi_j = 1$ at the corresponding node $(t_j, x_j)$ and zero otherwise. For the discrete initial velocity $v_{0h} \in V^h$, we approximate the system of primal and dual relations (9): Find a solution pair $(u_h, \lambda_h) \in V^h_{0,} \times \mathbb{R}^M$ such that

$$\begin{aligned} &u_h(t_h, x_h) \le L - x_h, \quad \lambda_h \le 0, \quad \lambda_h\big(u_h(t_h, x_h) - L + x_h\big) = 0 \quad \text{for } (t_h, x_h) \in \widetilde{Q}, \\ &\int_Q (-u_{ht}\phi_{ht} + u_{hx}\phi_{hx})\, dxdt = \int_0^L v_{0h}\phi_h\, dx\big|_{t=0} + \lambda_h \end{aligned} \tag{22}$$

for all basis functions $\phi_h \in V^h_{,0}$. In contrast to an integral approach providing for non-penetration within whole elements, the nodal enforcement of constraints in (22) imposes for non-penetrating both on an individual element as well as at the boundary. Here, $\lambda_h$ is referred to as a Lagrange multiplier compared to the contact force $\lambda$ in (1) and (2).

**Theorem 2.** *Let the complementary sets of active and inactive nodes be defined as*

$$\begin{aligned} \mathcal{A}(u_h, \lambda_h) &= \{(t_h, x_h) \in \widetilde{Q}: \quad r\lambda_h - u_h(t_h, x_h) + L - x_h < 0\}, \\ \mathcal{I}(u_h, \lambda_h) &= \{(t_h, x_h) \in \widetilde{Q}: \quad r\lambda_h - u_h(t_h, x_h) + L - x_h \ge 0\}, \end{aligned} \tag{23}$$

*for $r > 0$. Using (23), system (22) can be realized as an implicit variational equation for the primal variable on a linear subspace: Find $u_h \in V^h_{0,}$ such that*

$$u_h(t_h, x_h) = L - x_h \text{ on } \mathcal{A}(u_h, \lambda_h), \quad \int_Q (-u_{ht}\phi_{ht} + u_{hx}\phi_{hx})\, dxdt = \int_0^L v_{0h}\phi_h\, dx\big|_{t=0} \tag{24}$$

*for all test functions $\phi_h \in V^h_{,0}$ with $\phi_h(t_h, x_h) = 0$ on $\mathcal{A}(u_h, \lambda_h)$. In contrast, a dual variable (the Lagrange multiplier) $\lambda_h \in \mathbb{R}^M$ is defined such that*

$$\lambda_h = \begin{cases} r_h & \text{on } \mathcal{A}(u_h, \lambda_h), \\ 0 & \text{on } \mathcal{I}(u_h, \lambda_h), \end{cases} \tag{25}$$

*can be determined from the residual* $r_h \in \mathbb{R}^{\mathrm{DOF}}$ *as*

$$r_h = \int_Q (-u_{ht}\phi_{ht} + u_{hx}\phi_{hx})\,dxdt - \int_0^L v_{0h}\phi_h\,dx\big|_{t=0}. \tag{26}$$

**Proof.** According to the definition of active–inactive sets in (23) and complementarity conditions in (22), we have two options:

$$\begin{cases} u_h(t_h, x_h) - L + x_h = 0, & \lambda_h < 0 \quad \text{on } \mathcal{A}(u_h, \lambda_h), \\ u_h(t_h, x_h) - L + x_h \le 0, & \lambda_h = 0 \quad \text{on } \mathcal{I}(u_h, \lambda_h). \end{cases}$$

Therefore, relations (22) turns into (23)–(26) and vice versa. □

As a consequence of Theorem 2, we derive space-time iteration of the problems (23)–(26) over active sets, yielding a solution to the discretized primal–dual variational problem (22).

Some heuristics for stable implementation of Algorithm 1 are given, avoiding numerical instabilities and cycling.

**Algorithm 1:** *(ST-PDAS).*

**Initialization:** *set iteration number* $k = 0$ *and initialize active set* $\mathcal{A}^0 = \emptyset$.

**Iteration:** *solve the linear system: Find* $u_h^k \in V_{0,}^h$ *such that*

$$u_h^k(t_h, x_h) = L - x_h \text{ on } \mathcal{A}_h^k, \quad \int_Q (-u_{ht}^k\phi_{ht} + u_{hx}^k\phi_{hx})\,dxdt = \int_0^L v_{0h}\phi_h\,dx\big|_{t=0} \tag{27}$$

*for all* $\phi_h \in V_{,0}^h$ *with* $v_h = 0$ *on* $\mathcal{A}_h^k$*; compute the residual* $r_h^k \in \mathbb{R}^{\mathrm{DOF}}$*:*

$$r_h^k = \int_Q (-u_{ht}^k\phi_{ht} + u_{hx}^k\phi_{hx})\,dxdt - \int_0^L v_{0h}\phi_h\,dx\big|_{t=0} \tag{28}$$

*and the Lagrange multiplier* $\lambda_h^k \in \mathbb{R}^M$*:*

$$\lambda_h^k = \begin{cases} r_h^k & \text{on } \mathcal{A}_h^k, \\ 0 & \text{on } \mathcal{I}_h^k; \end{cases} \tag{29}$$

*update the active and inactive sets:*

$$\begin{aligned} \mathcal{A}_h^{k+1} &= \{(t_h, x_h) \in \widetilde{Q} : \quad r\lambda_h^k - u_h^k(t_h, x_h) + L - x_h < -\mathtt{tol}\}, \\ \mathcal{I}_h^{k+1} &= \{(t_h, x_h) \in \widetilde{Q} : \quad r\lambda_h^k - u_h^k(t_h, x_h) + L - x_h \ge -\mathtt{tol}\}. \end{aligned} \tag{30}$$

**Termination:** *stop if the iteration cycles, or the stopping condition holds:*

$$\mathcal{A}_h^{k+1} = \mathcal{A}_h^k. \tag{31}$$

- The factors are $r = 1$ and $\mathtt{tol} = 10^{-5}$ in the definition of active and inactive sets (30).
- The computational domain $Q$ is extended to $(0, T + 2h) \times (0, L)$ to fit the final time in the trial $V_{0,}^h$ and the test $V_{,0}^h$ spaces.
- At the contact boundary $\Gamma$, for extended grid points $\{t = T + h, x = L\}$, $\{t = T + 2h, x = L\}$, and for $t^* \in (0, T)$, where the inactive set meets the active

set (here $t^* = \tau$), we realize the Neumann condition $\lambda_h^k = u_{hx}^k = 0$ in (18) by using the finite difference defined as

$$u_h^k(t, L) - u_h^k(t, L - h) = 0 \quad \text{for } t \in \{t^*, T + h, T + 2h\}. \tag{32}$$

The finite difference approximation (32) for $t = t^*$ preserves iterates from instabilities happening near discontinuities.

- To avoid the instability of iteration (30) that becomes possible after collision for $k \geq 2$, we use re-initialization of the inactive set $\mathcal{I}_h^k$ with $\mathcal{I}_h^{k'}$, satisfying the monotony condition

$$\lambda_j^k = 0 \quad \text{for } j = 1, \ldots, \text{DOF such that } \mathcal{I}_j^{k-1} = \mathcal{I}_j^{k-2}. \tag{33}$$

The heuristic re-initialization (33) remedies the M-property of the stiffness matrix and prevents iterates from cycling without it during contact transitions.

- If the stopping condition (31) is attained, then $r\lambda_h^k < -\texttt{tol}$ on $\mathcal{A}_h^k$ and $u_h^k(t_h, x_h) - L + x_h \leq \texttt{tol}$ on $\mathcal{I}_h^k$ are guaranteed by (30). In the case of $\texttt{tol} \geq 0$ and $u_h^k(t_h, x_h) \leq L - x_h$ on $\mathcal{I}_h^k$, the iteration $(u_h^k, \lambda_h^k)$ solves the reference problems (23)–(26) exactly.

We justify the ST-PDAS algorithm on the analytical benchmark from Theorem 1.

## 5. Numerical Benchmark

For numerical tests, this study set the parameters of bar length $L = 1$, initial depth $H = 0.5$, and velocity $v_0 = 0.5$ such that the collision time $\tau = 1$ and the final time $T = 4$, as shown in Figure 3. According to Theorem 1 and Remark 3, the analytical solution to the primal–dual problem (9) is given for the displacement as

$$u(t, x) = \frac{1}{2} \begin{cases} t - 1 & \text{in } K_1 = \{0 \leq t \leq 4,\ 0 \leq x \leq 1 :\ x + t \leq 2\}, \\ 1 - x & \text{in } K_2 = \{0 \leq t \leq 4,\ 0 \leq x \leq 1 :\ x + t \geq 2,\ x - t \geq -2\}, \\ 3 - t & \text{in } K_3 = \{0 \leq t \leq 4,\ 0 \leq x \leq 1 :\ x - t \leq -2\}, \end{cases} \tag{34}$$

and for the Lagrange multiplier as

$$\lambda(t, x) = \begin{cases} 0 & \text{in } Q = \{0 < t < 4,\ 0 < x < 1\}, \\ \begin{cases} -0.5 & \text{if } 1 < t < 3 \\ 0 & \text{otherwise} \end{cases} & \text{on } \Gamma = \{0 < t < 4,\ x = 1\}. \end{cases} \tag{35}$$

After discretization of the collision problem in the finite element space $V^h$, the choice of the integer number $N$ determines the discrete parameters used in the following numerical tests. They are presented in Table 1: the mesh size $h$, the number of DOF in the closure $\mathrm{cl}(Q)$, the number $M$ of constrained nodes in $\widetilde{Q} = Q \cup \Gamma$, and the $M$/DOF ratio.

**Table 1.** Discrete parameters determined by the number $N$.

| N | h | DOF | M | M/DOF |
|---|---|---|---|---|
| 11 | 0.1 | 451 | 390 | 0.86 |
| 21 | 0.05 | 1701 | 1580 | 0.92 |
| 31 | 0.033 | 3751 | 3570 | 0.95 |
| 41 | 0.025 | 6601 | 6360 | 0.96 |
| 51 | 0.02 | 10,251 | 9950 | 0.97 |

According to Theorem 2, numerical solution to the corresponding discrete problem is computed with the help of Algorithm 1. For $N = 5$, an example solution is drawn

in Figure 4. Here, the displacement $u_h(t,x)$, velocity $u_{ht}(t,x)$, and gradient $u_{hx}(t,x)$ are presented over the uniform triangle grid in the left (a), middle (b), and right (c) plots, respectively, where the color of triangles varies according to its heights. The time and space derivatives in the latter two plots are discontinuous. The numerical solution $u_h$ computed at nodes $x_h$ is almost equal to the exact solution $u(x_h)$, with the error being less then $10^{-14}$. Indeed, the exact solution is given by a piecewise linear function on the partition $K_1$–$K_3$. Then, the piecewise linear interpolation differs only with respect to the elements crossing the interface $\Gamma_{23}$, which does not coincide with the diagonal grid.

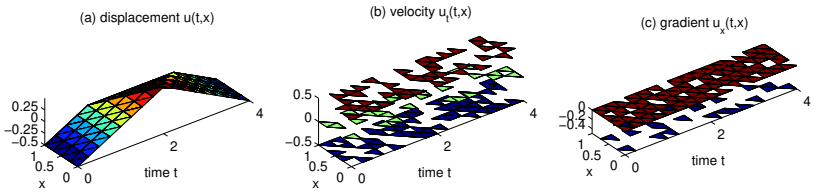


**Figure 4.** Example solution for $N = 5$: displacement $u_h$ (**a**), velocity $u_{ht}$ (**b**), and gradient $u_{hx}$ (**c**).

For physical consistency, the discrete energy is calculated from Formula (19) on the grid at equidistant time points $t_j = (j-1)h$ for $j = 1, \ldots, 4(N-1)+1$ such that

$$E_h(t_j) = \frac{1}{2} \sum_{i=1}^{3} \int_{K_i \cap \{t=t_j,\, x\in(0,1)\}} (u_{ht}^2 + u_{hx}^2)\, dx. \tag{36}$$

According to Corollary 1, the exact energy $E = 0.125$ is constant at all times. We measure the relative error with respect to the discrete $L^2$-norm as

$$\mathrm{Err}_h = \left\| \frac{E_h - E}{E} \right\| \times 100\ (\%). \tag{37}$$

The numerical energy $E_h$ computed from (36) and the relative energy error $\mathrm{Err}_h$ obtained by (37) are portrayed in the left (a) and right (b) plots of Figure 5, respectively. Here, one can observes piecewise constant values of $E_h$ with jumps at the times $t = 2$ and $t = 3$. These times correspond to the interface between regions $K_2$ and $K_3$ in the partition (37), which does not coincide with the diagonal grid. In contrary, the interface between regions $K_1$ and $K_2$ coincides with the diagonal grid, and energy at the time $t = 1$ is continuous without jump. The curves $E_h$ are visually indistinguishable from $E$ for $t < 2$ and $t > 3$; otherwise, they tend to $E$ when decreasing the step size $h$. The order of accuracy is estimated to be 1.5. The convergence rate is super-linear, that is, inherent for SSN methods.

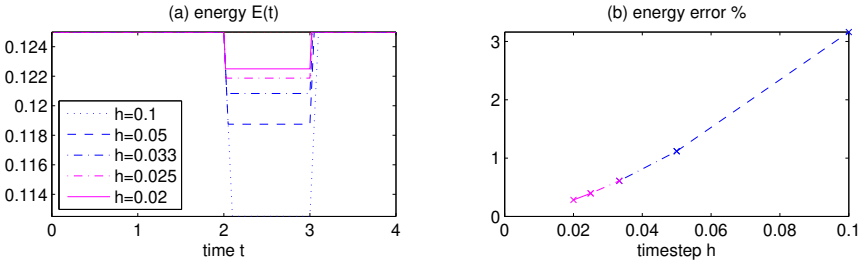


**Figure 5.** The discrete energy $E_h$ (**a**) and relative energy error $\mathrm{Err}_h$ (**b**).

Finally, the convergence behavior of the ST-PDAS algorithm is demonstrated. For $N = 51$, implying about $10^4$ constrained nodes, Algorithm 1 terminates successfully with $\mathcal{A}_h^{k+1} = \mathcal{A}_h^k$ at the final $k = 4$ iterate. The iteration history of active sets $\mathcal{A}_h^0$–$\mathcal{A}_h^{k+1}$ is shown in the dark color over $\widetilde{Q}$ in Figure 6. Here, we realize the Neumann condition (32) and apply the monotony condition (33) by re-initializing the inactive set $\mathcal{I}_h^2$ with $\mathcal{I}_h^{2'}$. Namely,

$\lambda_j^2 = 0$ is set for the nodes $j$ where the both previous iterates $\mathcal{I}_j^1 = \mathcal{I}_j^0$ were inactive. Here, one can observe at iterates 1 and 2 that the active sets $\mathcal{A}_h^1$ and $\mathcal{A}_h^2$ are bounded by lines $x + t = 3$ and $x + t = 2$, where the latter is characteristic, but the former is not.

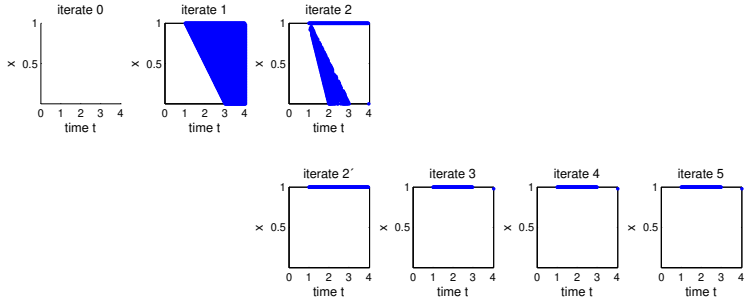


**Figure 6.** ST-PDAS iterates $\mathcal{A}_h^0$–$\mathcal{A}_h^5$ of the active set as $N = 51$.

We have observed the same behavior of active sets for all numbers $N$ tested. For illustration purposes, the iterates of the displacement $u_h^0$–$u_h^4$ in $\mathrm{cl}(Q)$ are shown in Figure 7 as $N = 3$. For $N = 5$, the iterates of the Lagrange multiplier $\lambda_h^0$–$\lambda_h^4$ over $\widetilde{Q}$ are presented in Figure 8. Here various colors are used for visualization reason to distinguish between portions of the reference rectangle $Q$.

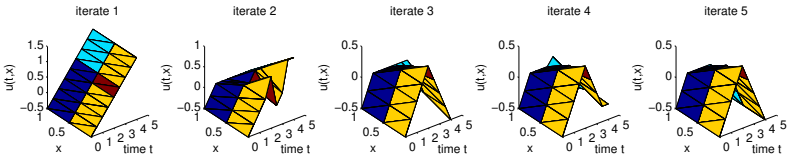


**Figure 7.** ST-PDAS iterates $u_h^0$–$u_h^4$ of the displacement as $N = 3$.

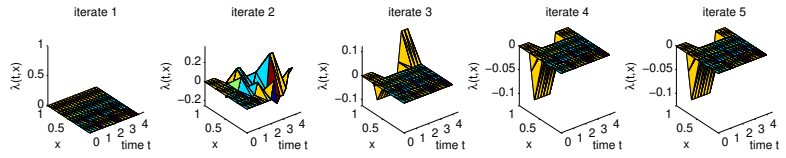


**Figure 8.** ST-PDAS iterates $\lambda_h^0$–$\lambda_h^4$ of the Lagrange multiplier as $N = 5$.

## 6. Concluding Remarks

A space-time method of finite-element approximation has been developed and endowed with a primal–dual active set iteration treating unilateral constraints in two dimensions. The ST-PDAS algorithm has been tested for an analytical benchmark of a rigid obstacle collided by an elastic bar, which is characterized by a discontinuous velocity. The numerical tests on a uniform triangular grid converge in few iterations when processing some heuristic conditions before and after collision and provided by re-initialization. On grid points, the numerical solution is visually indistinguishable from the exact solution, and the energy converges super-linearly under grid refinement. If the initial velocity of the bar is $v_0 \leq 1$, then the analytical solution is given by a piecewise linear function.

From the physical point of view, at time $t = \tau$, the bar collides with the obstacle at its upper end. An elastic wave propagates through the bar with a velocity 1 and reaches its opposite end when moving with a kinematic velocity $v_0 \leq 1$. Otherwise, the bar lower end

reaches the obstacle before then at the elastic wave. For $v_0 > 1$, there is a known bounce effect, which might be a subject of future research.

**Funding:** This research received no external funding.

**Data Availability Statement:** The data are contained within the article.

**Acknowledgments:** The author acknowledges the financial support by the University of Graz.

**Conflicts of Interest:** The author declares no conflicts of interest.

## References

1. Aguirregabiria, J.M.; Hernández, A.; Rivas, M. Falling elastic bars and springs. *Am. J. Phys.* **2007**, *75*, 583–587. https://doi.org/10.1119/1.2733680.
2. Younis, M.I. *MEMS Linear and Nonlinear Statics and Dynamics*; Springer: New York, NY, USA, 2011. https://doi.org/10.1007/978-1-4419-6020-7.
3. He, J.H. Periodic solution of a micro-electromechanical system. *Facta Univ. Ser. Mech. Eng.* **2024**, *22*, 187–198. https://doi.org/10.22190/FUME240603034H.
4. Gwinner, J.; Jadamba, B.; Khan, A.A.; Raciti, F. *Uncertainty Quantification in Variational Inequalities: Theory, Numerics, and Applications*; Chapman and Hall/CRC: New York, NY, USA, 2021. https://doi.org/10.1201/9781315228969.
5. Migórski, S.; Ochal, A.; Sofonea, M. *Nonlinear Inclusions and Hemivariational Inequalities: Models and Analysis of Contact Problems*; Springer: New York, NY, USA, 2013. https://doi.org/10.1007/978-1-4614-4232-5.
6. Lebeau, G.; Schatzman, M. A wave problem in a half-space with a unilateral constraint at the boundary. *J. Differ. Equ.* **1984**, *53*, 309–361. https://doi.org/10.1016/0022-0396(84)90030-5.
7. Laursen, T.A. *Computational Contact and Impact Mechanics*; Springer: Berlin/Heidelberg, Germany, 2003. https://doi.org/10.1007/978-3-662-04864-1.
8. Wriggers, P. *Computational Contact Mechanics*; Springer: Berlin/Heidelberg, Germany, 2006. https://doi.org/10.1007/978-3-540-32609-0.
9. Chouly, F.; Hild, P.; Renard, Y. *Finite Element Approximation of Contact and Friction in Elasticity*; Birkhäuser: Cham, Switzerland, 2023. https://doi.org/10.1007/978-3-031-31423-0.
10. Haslinger, J.; Neittaanmäki, P. *Finite Element Approximation for Optimal Shape, Material and Topology Design*; Wiley: Chichester, UK, 1996.
11. Gwinner, J.; Stephan, E.P. *Advanced Boundary Element Methods. Treatment of Boundary Value, Transmission and Contact Problems*; Springer: Cham, Switzerland, 2018. https://doi.org/10.1007/978-3-319-92001-6.
12. Steinbach, O.; Wendland, W.L. Boundary element methods for contact problems. In *Advanced Multibody System Dynamics*; Schiehlen, W., Ed.; Springer: Dordrecht, The Netherlands, 1993; pp. 433–438. https://doi.org/10.1007/978-94-017-0625-4_31.
13. Bauer, E.; Kovtunenko, V.; Krejčí, P.; Monteiro, G.; Paoli, L.; Petrov, A. Non-convex sweeping processes in contact mechanics. *Nonlinear Anal. Real World Appl.* **2025**, p. 104456. https://doi.org/10.1016/j.nonrwa.2025.104456.
14. Kashiwabara, T.; Itou, H. Unique solvability of a crack problem with Signorini-type and Tresca friction conditions in a linearized elastodynamic body. *Phil. Trans. R. Soc. A* **2022**, *380*, 20220225. https://doi.org/10.1098/rsta.2022.0225.
15. Piersanti, P.; White, K.; Dragnea, B.; Temam, R. A three-dimensional discrete model for approximating the deformation of a viral capsid subjected to lying over a flat surface in the static and time-dependent case. *Anal. Appl.* **2022**, *20*, 1159–1191. https://doi.org/10.1142/S0219530522400024.
16. Rudoy, E.M.; Sazhenkov, S.A. The homogenized dynamical model of a thermoelastic composite stitched with reinforcing filaments. *Phil. Trans. R. Soc. A* **2024**, *382*, 20230304. https://doi.org/10.1098/rsta.2023.0304.
17. Efendiev, M.; Vougalter, V. On the well-posedness of some model with the cubed Laplacian arising in the Mathematical Biology. *arXiv* **2025**, arXiv:2504.10628. https://doi.org/10.48550/arXiv.2504.10628.
18. Egger, H.; Fellner, K.; Pietschmann, J.F.; Tang, B.Q. Analysis and numerical solution of coupled volume-surface reaction-diffusion systems with application to cell biology. *Appl. Math. Comput.* **2018**, *226*, 351–367. https://doi.org/10.1016/j.amc.2018.04.031.
19. Liu, W.; Borikarnphanichphaisal, K.; Song, J.; Vasilieva, O.; Svinin, M. Safe 3D coverage control for multi-agent systems. *Actuators* **2025**, *14*, 186. https://doi.org/10.3390/act14040186.
20. Dirani, N.; Monasse, L. An explicit pseudo-energy conservative scheme for contact between deformable solids. *Int. J. Numer. Meth. Engng.* **2024**, *125*, e7395. https://doi.org/10.1002/nme.7395.
21. Doyen, D.; Ern, A.; Piperno, S. Time-integration schemes for the finite element dynamic Signorini problem. *SIAM J. Sci. Comput.* **2011**, *33*, 223–249. https://doi.org/10.1137/100791440.
22. Dabaghi, F.; Krejčí, P.; Petrov, A.; Pousin, J.; Renard, Y. A weighted finite element mass redistribution method for dynamic contact problems. *J. Comput. Appl. Math.* **2019**, *345*, 338–356. https://doi.org/10.1016/j.cam.2018.06.030.

23. Dabaghi, F.; Petrov, A.; Pousin, J.; Renard, Y. A robust finite element redistribution approach for elastodynamic contact problems. *Appl. Numer. Math.* **2016**, *103*, 48–71. https://doi.org/10.1016/j.apnum.2015.12.004.
24. Khenous, H.B.; Laborde, P.; Renard, Y. Comparison of two approaches for the discretization of elastodynamic contact problems. *C. R. Acad. Sci. Paris Ser. I* **2006**, *342*, 791–796. https://doi.org/10.1016/j.crma.2006.03.011.
25. Paoli, L.; Schatzman, M. A numerical scheme for impact problems I: The one-dimensional case. *SIAM J. Numer. Anal.* **2002**, *40*, 702–733. https://doi.org/10.1137/S0036142900378728.
26. Newmark, N.M. A method of computation for structural dynamics. *J. Eng. Mech. Div.* **1959**, *85*, 67–94. https://doi.org/10.1061/JMCEA3.0000098.
27. Hilber, H.M.; Hughes, T.J.R.; Taylor, R.L. Improved numerical dissipation for time integration algorithms in structural dynamics. *Earthq. Eng. Struct. Dyn.* **1977**, *5*, 283–292. https://doi.org/10.1002/eqe.4290050306.
28. Kovtunenko, V.A.; Atlasiuk, O.M. Poroelastic medium with non-penetrating crack driven by hydraulic fracture: FEM approximation using HHT-$\alpha$ and semi-smooth Newton methods. *Algorithms* **2025**, *submitted for publication*.
29. Kovtunenko, V.A.; Renard, Y. Convergence analysis of semi-smooth Newton method for mixed FEM approximations of dynamic two-body contact and crack problems. *J. Comput. Appl. Math.* **2025**, *471*, 116722. https://doi.org/10.1016/j.cam.2025.116722.
30. Kovtunenko, V.A.; Renard, Y. FEM approximation of dynamic contact problem for fracture under fluid volume control using HHT-$\boldsymbol{\alpha}$ and semi-smooth Newton methods. *Appl. Numer. Math.* **2025**, *218*, 148–158. https://doi.org/10.1016/j.apnum.2025.07.009.
31. Khludnev, A.; Kovtunenko, V. *Analysis of Cracks in Solids*; Advances in Fracture Mechanics Series; WIT-Press: Southampton, UK; Boston, MA, USA, 2000; Volume 6.
32. Khludnev, A.M.; Sokolowski, J. *Modeling and Control in Solid Mechanics*; Birkhäuser: Basel, Switzerland, 1997. https://doi.org/10.1007/978-3-0348-8984-1.
33. Fernando, M.P.; Mallikarjunaiah, S.M. An AT1 phase-field framework for quasi-static anti-plane shear fracture: Unifying $\xi$-based adaptivity and nonlinear strain energy density function. *arXiv* **2025**, arXiv:2506.23249. https://doi.org/10.48550/arXiv.2506.23249.
34. Itou, H.; Kovtunenko, V.; Rajagopal, K. The Boussinesq flat-punch indentation problem within the context of linearized viscoelasticity. *Int. J. Eng. Sci.* **2020**, *151*, 103272. https://doi.org/10.1016/j.ijengsci.2020.103272.
35. Khludnev, A.M.; Kovtunenko, V.A.; Tani, A. Evolution of a crack with kink and non-penetration. *J. Math. Soc. Japan* **2008**, *60*, 1219–1253. https://doi.org/10.2969/jmsj/06041219.
36. Nikolaeva, N. Junction problem for elastic Timoshenko inclusions in elastic bodies with a crack. *J. Appl. Ind. Math.* **2024**, *18*, 775–787. https://doi.org/10.1134/S1990478924040124.
37. Ghosh, S.; Bhatta, D.; Mallikarjunaiah, S.M. Computational insights into orthotropic fracture: crack-tip fields in strain-limiting materials under non-uniform loads. *arXiv* **2025**, arXiv:2507.01150. https://doi.org/10.48550/arXiv.2507.01150.
38. Kovtunenko, V.A.; Lazarev, N.P. Variational inequality for a Timoshenko plate contacting at the boundary with an inclined obstacle. *Phil. Trans. R. Soc. A* **2024**, *382*, 20230298.
39. Popova, T. Numerical solution of the equilibrium problem for a two-dimensional elastic body with a delaminated rigid inclusion. *Lobachevskii J. Math.* **2024**, *45*, 5402–5413. https://doi.org/10.1134/S1995080224606660.
40. Alekseev, G.; Spivak, Y. Optimization-based numerical analysis of three-dimensional magnetic cloaking problems. *Comput. Math. Math. Phys.* **2021**, *61*, 212–225. https://doi.org/10.1134/S0965542521020032.
41. Fellner, K.; Kovtunenko, V.A. A singularly perturbed nonlinear Poisson–Boltzmann equation: uniform and super-asymptotic expansions. *Math. Meth. Appl. Sci.* **2015**, *38*, 3575–3586. https://doi.org/10.1002/mma.3593.
42. Lyu, J.H.; Lin, T.C. Asymptotic analysis of boundary layer solutions to Poisson–Boltzmann type equations in general bounded smooth domains. *arXiv* **2025**, arXiv:2506.20953. https://doi.org/10.48550/arXiv.2506.20953.
43. Ito, K.; Kunisch, K. *Lagrange Multiplier Approach to Variational Problems and Applications*; SIAM: Philadelphia, PA, USA, 2008. https://doi.org/10.1137/1.9780898718614.
44. Hintermüller, M.; Kovtunenko, V.A.; Kunisch, K. Generalized Newton methods for crack problems with non-penetration condition. *Numer. Meth. Partial Differ. Equ.* **2005**, *21*, 586–610. https://doi.org/10.1002/num.20053.
45. Hintermüller, M.; Kovtunenko, V.A.; Kunisch, K. A Papkovich–Neuber-based numerical approach to cracks with contact in 3D. *IMA J. Appl. Math.* **2009**, *74*, 325–343. https://doi.org/10.1093/imamat/hxp017.
46. Abide, S.; Barboteu, M.; Cherkaoui, S.; Danan, D.; Dumont, S. Inexact primal–dual active set method for solving elastodynamic frictional contact problems. *Comput. Math. Appl.* **2021**, *82*, 36–59. https://doi.org/10.1016/j.camwa.2020.11.017.
47. Nguyen, V.A.T.; Abide, S.; Barboteu, M.; Dumont, S. An improved normal compliance method for non-smooth contact dynamics. *Banach Center Publ.* **2024**, *124*, 191–217. https://doi.org/10.4064/bc127-9.
48. Kovtunenko, V.A. Space-time finite element based primal-dual active set method for the non-smooth problem of impact of rigid obstacle by elastic bar. *Comput. Math. Model.* **2025**, *36*. https://doi.org/10.1007/s10598-025-09629-9.
49. Kovtunenko, V.A.; Petrov, A.; Renard, Y. Space-time FEM solution of dynamic contact problem with discontinuous velocity for multiple impact of deformed bar using PDAS method. *Math. Meth. Appl. Sci.* **2025**, *submitted for publication*.

50. Zank, M. *Inf-Sup Stable Space-Time Methods for Time-Dependent Partial Differential Equations*; Verlag der TU Graz: Graz, Austria, 2020.
51. Zlotnik, A. Convergence rate estimates of finite-element methods for second order hyperbolic equation. In *Numerical Methods and Applications*; Marchuk, G.I., Ed.; CRC Press: Boca Raton, FL, USA, 1994; pp. 155–220. https://doi.org/10.1201/9780203711200.